J. Shanghai Jiao Tong Univ. (Sci.), 2022, 27(3): 356-364
https://doi.org/10.1007/s12204-021-2321-5

Numerical Simulation of the Flow in a Waterjet Intake Under Different Motion Conditions

XU Huili[a] (许慧丽), *ZOU Zaojian*[a,b*] (邹早建)
(a. School of Naval Architecture, Ocean and Civil Engineering; b. State Key Laboratory of Ocean Engineering, Shanghai Jiao Tong University, Shanghai 200240, China)

Abstract: By solving the three-dimensional incompressible Reynolds-averaged Navier-Stokes equations, numerical simulations of the viscous flow within a flush type intake duct of a waterjet under different motion conditions are carried out. Therein, the effects of the steering and reversing unit as well as the impeller shaft on the flow field are taken into account. The numerical results show that the static pressure under backward conditions with the reversing jet flow is the lowest, and the cavitations are most likely to occur within the intake duct. The flow field under forward conditions is less uniform because of the shaft, while the velocity uniformity under backward conditions is improved. The shaft rotation causes an asymmetric secondary flow above the shaft under all conditions. The pressure contours under backward conditions with the reversing jet flow are sensitive to the presence of the shaft. This study can provide some references for the design optimization of waterjet propulsion system.
Key words: waterjet, intake duct, viscous flow, numerical simulation
CLC number: U 661.31 **Document code:** A

0 Introduction

In the last decades, waterjet propulsion has found a considerable application on a wide range of high-speed marine vessels by virtue of many advantages. Waterjet is recommended as a substitute of marine propulsion device for traditional screw propellers to reduce noise and vibration as well as avoid cavitation and related problems at high speeds. In addition, its propulsive efficiency is much higher especially when the vessel speed exceeds 30 kn. The manoeuvrability of a waterjet propulsion system is potentially very good because of the deflector units, which direct the water flow and hence introduce turning moment. All these have contributed to the growing application and study of waterjet propulsion system.

The operation principle of the waterjet is that the water is drawn through a ducting system by an internal pump and expelled aft at high velocity[1]. To provide a better waterjet performance, the intake duct is required to deliver sufficient water to the pump unit to propel the vessel and prevent flow separation along the curved duct. Therefore, the research on the flow features within the waterjet intake duct is of great importance, and a number of studies have been carried out. For instance, Verbeek and Bulten[2] found that approximately 7%—9% of the total power loss occurred within the intake duct. Ding and Wang[3] introduced a new method to acquire the flow loss of inlet duct based on the momentum flux method and the standard locations recommended by the Specialist Committee on Validation of Waterjet Test Procedures of International Towing Tank Conference[4-5]. Von Ellenrieder[6] performed free running trials of an unmanned surface vehicle to investigate the effects of cross flow at the inlet of the waterjets.

The flexible manoeuvrability of a waterjet propulsion system comes from the steering and reversing unit, a mechanically or hydraulically actuated device used to direct the flow and hence produce turning or retarding forces on the vessel through the change in the direction of jet momentum. Both the brake time and the stopping distance of a waterjet propelled vehicle are much shorter than those of a vehicle propelled by traditional screw propeller. Many patents have been issued on the optimization of the waterjet steering and reversing unit. However, previous works did not pay much attention to its hydrodynamic characteristics, i.e., the water flow within and around the waterjet under different steering

Received: 2019-05-13 **Accepted:** 2019-11-11
Foundation item: the Fund of Key Laboratory of Waterjet Propulsion Technology of MARIC (No. 61422230301162223010)
∗**E-mail:** zjzou@sjtu.edu.cn

conditions.

The developments in computer hardware and numerical algorithms have led to an enormous increase in the use of computational fluid dynamics (CFD) methods for performance evaluation of marine propulsion systems. Nowadays, the analysis of the flow through the waterjet duct system as well as the design optimization of the intake geometry based on CFD calculations is becoming a common practice[7-8]. The characteristics of flow within the waterjet ducts have been investigated by many researchers. Park et al.[9] solved the Reynolds-averaged Navier-Stokes (RANS) equations to gain the detailed flow information of a flush type waterjet intake, and systematically compared the calculation results with experimental data for code validation. Bulten[10-11] performed a detailed investigation both experimentally and numerically, and the computed results using CFD code with a multiple frames of reference (MFR) method agreed well with the experimental data. Eslamdoost[12] studied the physical mechanism behind waterjet-hull interaction based on RANS simulations, and developed a numerical method for estimating the gross thrust of a waterjet driven hull.

In this study, the flow field within a flush type of waterjet intake under different motion conditions is numerically simulated by solving the three-dimensional (3D) RANS equations. Therein, the effects of the steering and reversing unit as well as the impeller shaft are taken into account. Systematic computations are performed at different jet velocity ratios. Significant features of the flow within the intake duct, especially near the impeller plane and the waterjet intake inlet, are presented and analyzed.

1 Simulated Scenarios

Waterjet intake is typically classified into two types: ram and flush types. Ram intakes are often used on hydrofoil crafts, while flush intakes have a wider range of application on planing crafts, mono-hull crafts, and catamarans. In the present study, a flush type of waterjet intake duct model is selected for numerical simulations, as shown in Fig. 1, where D is the diameter of the duct and $D = 0.272\,\mathrm{m}$. Experimental results of this model can be found in Jung et al.[13].

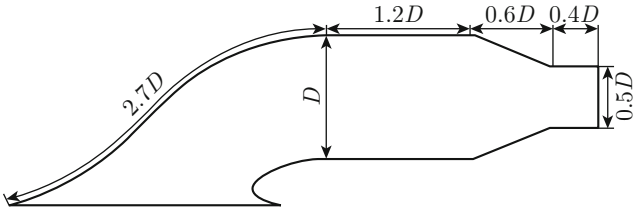

Fig. 1 A flush type of waterjet intake duct model

The flow field inside and around the waterjet propulsion system is quite different from that of screw propellers when vessels move backward, obliquely or turn. The flow around the propellers of traditional propelled ships has the same direction as that around the hull, but the flow inside the waterjet keeps the original direction while the flow around the waterjet driven hull changes direction under different motion conditions. When the effects of redirected jet flow and the shaft rotation are taken into account, the flow field within the waterjet intake becomes more complicated. In the present study, four motion conditions are chosen for comparison and analysis, as given in Table 1.

Table 1 Simulation cases under different motion conditions

Case	Motion condition	Shaft condition
1-A	Forward	Without
1-B	Forward	Stationary
1-C	Forward	Rotating
2-A	Backward	Without
2-B	Backward	Stationary
2-C	Backward	Rotating
3-A	Backward with reversing flow	Without
3-B	Backward with reversing flow	Stationary
3-C	Backward with reversing flow	Rotating
4-A	Oblique	Without
4-B	Oblique	Stationary
4-C	Oblique	Rotating

For each condition, computations are carried out at three jet velocity ratio (JVR) values: JVR = 6, 7, 8 (same values as in the experiments[13]), which is defined as

$$\mathrm{JVR} = \frac{V_\mathrm{j}}{V_\infty}, \tag{1}$$

where V_j is the jet velocity at nozzle exit, and V_∞ is the vessel velocity.

Case 1 and Case 2 are chosen to study the differences of the intake duct performances between forward and backward conditions. Besides, the flow within the intake duct under backward conditions with and without reversing flow is different. Simulation results of Case 2 and Case 3 are compared to reveal this difference.

During oblique motion, because of the fixed waterjet intake duct geometry and transverse flow across the hull, the flow sucked in through the inlet does not follow the patterns of forward motion conditions. The simulated results of Case 4 are presented to show the flow characteristics in oblique motion.

In addition, the presence of impeller shaft and its rotation are important influence factors to the flow field and should also be taken into account. Computations are performed with and without these effects for all motion conditions, and the results are compared.

2 Numerical Method

2.1 Governing Equations

The flow in the waterjet system is a 3D flow of incompressible viscous fluid, which is governed by the Reynolds-averaged continuity equation and the RANS equations:

$$\frac{\partial u_i}{\partial x_i} = 0, \tag{2}$$

$$\rho\frac{\partial u_i}{\partial t} + \rho u_j\frac{\partial u_i}{\partial x_j} = -\frac{\partial p}{\partial x_i} + \frac{\partial}{\partial x_j}\left(\mu\frac{\partial u_i}{\partial x_j} - \rho\overline{u_i'u_j'}\right) + S_i, \quad i = 1,2,3, \tag{3}$$

where x_i and x_j are the components of coordinate system, u_i and u_j are the mean velocity components, p is the mean pressure, ρ is the fluid density, μ is the viscosity coefficient, $-\rho\overline{u_i'u_j'}$ is the Reynolds stress tensor, and S_i is the source term.

The standard k-ε turbulence model is one of the most commonly used models in numerical simulation, which is adopted in the present work to close the governing equations:

$$\frac{\partial(\rho k)}{\partial t} + \frac{\partial(\rho k u_j)}{\partial x_j} = \frac{\partial}{\partial x_j}\left[\left(\mu + \frac{\mu_t}{\sigma_k}\right)\frac{\partial k}{\partial x_j}\right] + G_k - \rho\varepsilon, \tag{4}$$

$$\frac{\partial(\rho\varepsilon)}{\partial t} + \frac{\partial(\rho\varepsilon u_j)}{\partial x_j} = \frac{\partial}{\partial x_j}\left[\left(\mu + \frac{\mu_t}{\sigma_\varepsilon}\right)\frac{\partial \varepsilon}{\partial x_j}\right] + \frac{C_{1\varepsilon}\varepsilon}{k}G_k - C_{2\varepsilon}\rho\frac{\varepsilon^2}{k}, \tag{5}$$

where k is the turbulent kinetic energy, ε is the dissipation rate of turbulent kinetic energy, μ_t is the turbulent viscosity, and

$$G_k = \mu_t\left(\frac{\partial u_i}{\partial x_j} + \frac{\partial u_j}{\partial x_i}\right)\frac{\partial u_i}{\partial x_j}, \tag{6}$$

$$C_{1\varepsilon} = 1.44, \quad C_{2\varepsilon} = 1.92, \quad \sigma_k = 1.0, \quad \sigma_\varepsilon = 1.3. \tag{7}$$

2.2 Computational Domain and Boundary Conditions

The computational domains for various motion conditions without the impeller shaft are shown in Fig. 2. For each condition, the computational domain is composed of the intake duct and a cuboid with the dimensions of $20D \times 10D \times 8D$. For all simulation cases, the duct model is placed at the center of the top side of the computational domain. Structured hexahedral cells are generated around the waterjet duct. In order to generate a grid system with high quality, an O-type mesh is applied in the duct, and special attention is paid to the reversing flow and the shaft regions. Meanwhile, fine mesh is used around the inlet area where the flow field changes dramatically. Making tradeoff between the computation efficiency and accuracy, the standard k-ε turbulence model along with the standard wall function is adopted. The final multi-block volume

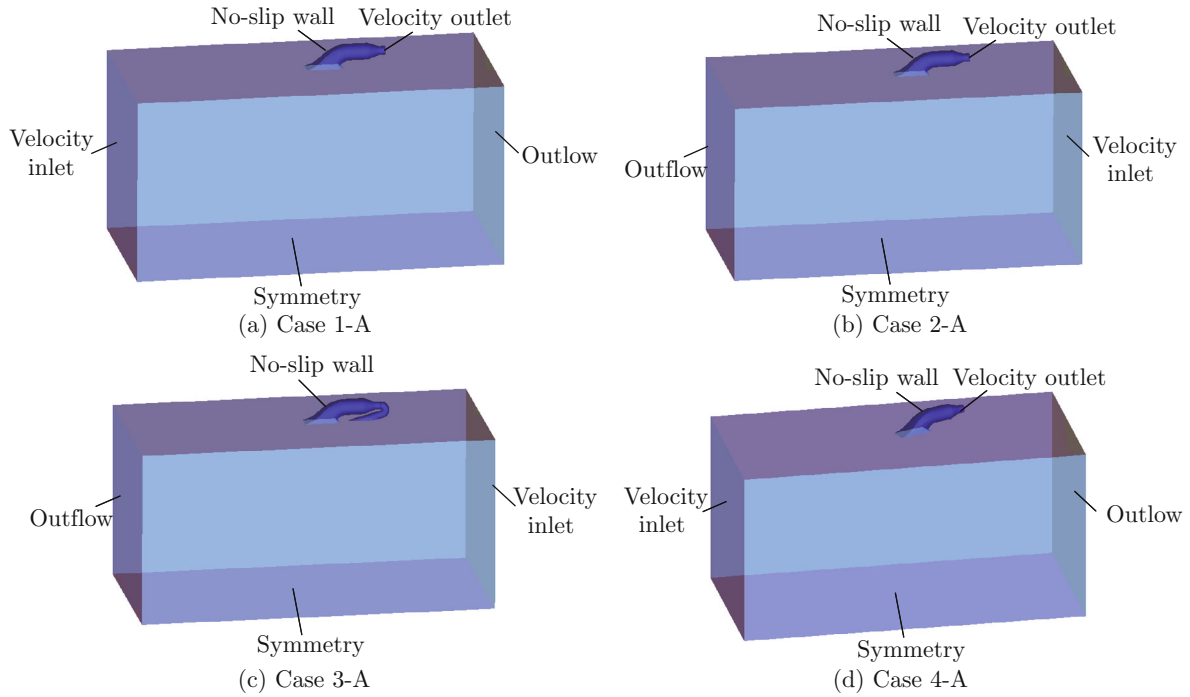

Fig. 2 Computational domains

mesh contains approximately one million hexagonal cells, with which the simulation results agree well with experimental data. The whole grid system and the grid for the intake duct are shown in Fig. 3.

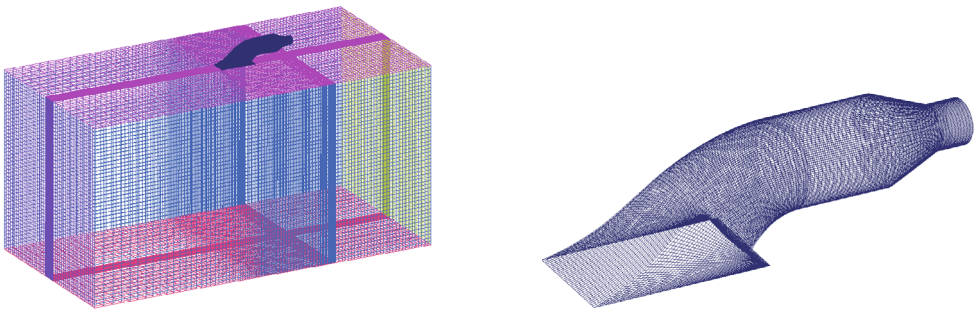

(a) Whole grid system of Case 1-A (b) Grid for intake duct

Fig. 3 Grid system

The boundary conditions for the computational domain can be divided into four major groups. ① At the inlet plane, an inlet velocity boundary condition of 4 m/s is imposed. This type of boundary condition requires a prescription of the three velocity components and values for the turbulence model. For forward and oblique motion conditions, the left plane of the domain is the inlet boundary; while in the cases of backward motions, the right plane is the inlet boundary. ② Another velocity-inlet boundary condition is imposed at the nozzle exit plane. Here the outflow velocity is adjusted for different JVR values to match the corresponding experiments. As the flow in the computational domain separates into two directions, the second type of boundary condition is applied on the outlet plane, which is opposite to the inlet plane. In this work, a constant pressure boundary condition is imposed on the outlet plane, which allows a non-uniform outflow velocity distribution. ③ The third type of boundary condition is the no-slip wall condition. It is imposed on the surface of the waterjet duct system, and on the boundary of the stream tube of reversing jet flow as a simplified duct flow model. In the cases with the rotating shaft of 0.04 m diameter and 4 000 r/min, a rotating wall boundary condition is applied on the shaft surface. As the focus is on the effect of inflow from different directions within the waterjet, the boundary layer flow is neglected in the present work. ④ The last type of boundary condition is the symmetry condition, which is imposed on the surfaces of the top, bottom, front and back sides of the computational domain.

2.3 Numerical Solutions

The numerical simulations are performed by using the CFD code ANSYS-Fluent. It solves the governing equations using a cell-centered finite volume method (FVM). The governing equations are discretized by FVM. The pressure-related term is discretized with the standard discretization scheme, while the other terms are discretized by the second-order upwind scheme to enhance the computation accuracy. The SIMPLEC algorithm is applied to solve the velocity-pressure coupling problem. Different user defined functions (UDFs) are used to control different zones in the computational domain in order to maintain proper mesh quality with good accuracy and computation speed at the same time.

3 Results and Discussion

Numerical results of all the simulations are presented and analyzed. The locations of the pressure tabs are numbered from the intake entrance to the nozzle exit, as shown in Fig. 4.

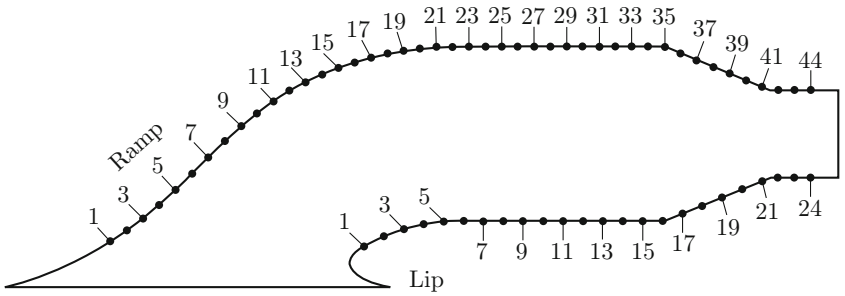

Fig. 4 Locations of pressure tabs

3.1 Forward and Backward Conditions

The previous study[14] showed that the simulation results of Case 1-A agree well with the available data of the wind tunnel experiments carried out by Jung et al.[13], which verifies the correctness and effectiveness of the numerical method applied in the present work.

Figure 5 shows the differences of surface pressure coefficients C_p along the duct between forward and backward conditions without the shaft at three JVR values (JVR = 6, 7, 8). For easy comparison, the pressure coefficient is the absolute value defined as

$$C_p = -\frac{2(p - p_\infty)}{\rho V_\infty^2}, \tag{8}$$

where p_∞ is the ambient pressure.

It can be seen from Fig. 5 that the pressure rapidly increases from tab number 35 and reaches the peak at the 42nd tab on the ramp side, and a similar tendency exists on the lip side. The sudden pressure change results from the bottleneck effect of the converging section of the nozzle area. It is obvious that the pressure coefficients on the ramp side under backward conditions are lower than those under forward conditions before the 10th tab, which probably results from the effect of the reversing jet flow; but they become higher after that and keep increasing while remaining steady under forward conditions. The surface pressure coefficients on the lip side in Case 2-A are also higher than those in Case 1-A, and meanwhile, higher than those on the ramp side. These results indicate lower static pressure under backward conditions for the impeller and worse operation condition for the waterjet system. It can be found that larger JVR values result in larger C_p along the duct, which is due to the faster flow at larger JVR.

In Fig. 6, the simulation results of cases with and without the shaft at JVR=8 are compared to investigate the effects of the shaft. An obvious disparity can be found between Case 1-A and Case 1-B from the 8th tab to 12th tab on the ramp side. There is little obvious difference found on the lip side even with larger scale of result curves, as shown in Fig. 6(b), indicating that the surface pressure on the lip wall is not sensitive to the presence of the shaft. However, it should be noted that the pressure distributions only present the characteristics of part of the flow field within the intake duct. The tendency of the surface pressure coefficients under backward conditions is similar to that under forward conditions on both ramp and lip sides.

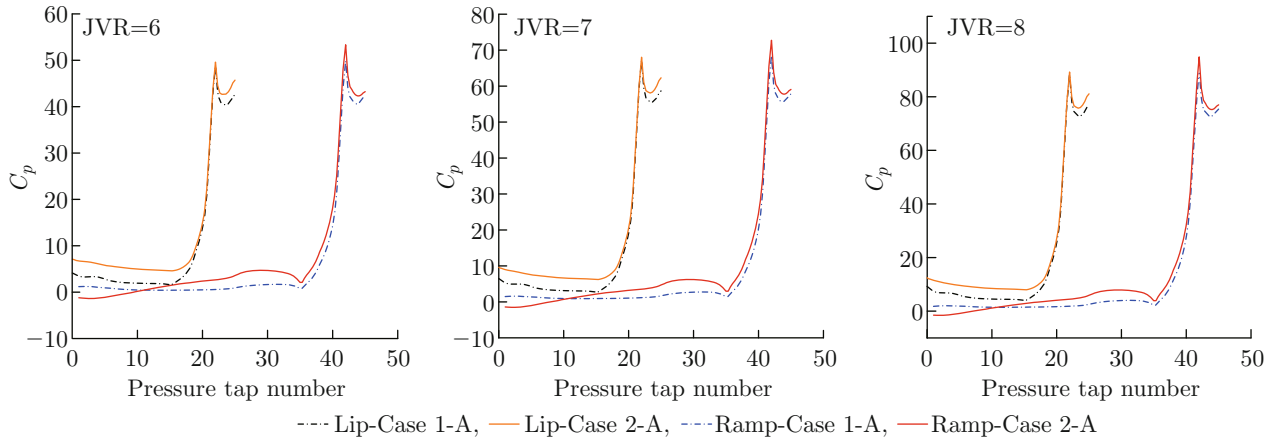

Fig. 5 Pressure distribution under forward and backward conditions

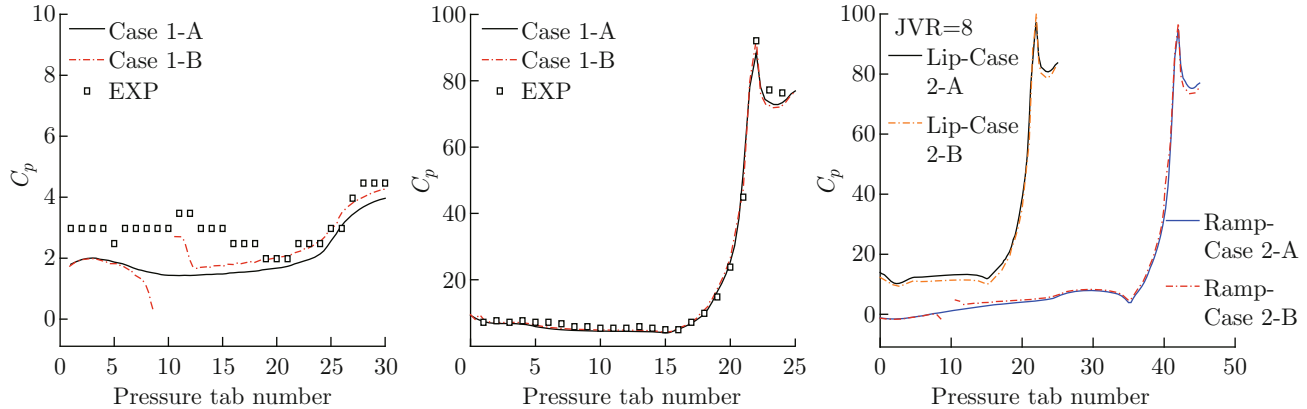

(a) Ramp side of Case 1-A and 1-B (b) Lip side of Case 1-A and 1-B (c) Case 2-A and 2-B

Fig. 6 Pressure distribution affected by stationary shaft at JVR=8

In terms of better waterjet performance, the flow delivered to the pump unit should be as uniform as possible. The non-uniformity of flow field is computed for each condition to assess the influence of the shaft, which can be defined by

$$\xi = \frac{1}{Q}\int_A \left|u - \overline{U}\right| \mathrm{d}A, \tag{9}$$

where Q is the flow rate, A is the area of cross section, and $\overline{U}$ is the mean velocity at the impeller plane. Larger value of ξ means less uniform flow field.

Figure 7 gives the non-uniformity of flow at the impeller plane under forward and backward conditions with and without the shaft. It can be seen that the values of ξ in Case 2 are much larger than those in Case 1, indicating that the flow field is more non-uniform under backward conditions. The presence of the shaft results in larger ξ under forward conditions because it blocks the streamlines within the waterjet duct. However, the results of Case 2-B are lower than those of the cases without the shaft, indicating that the shaft helps to improve the uniformity of the flow field under backward conditions. In addition, the non-uniformities of all cases become lower as JVR increases, as the velocity distribution becomes more uniform with faster flow.

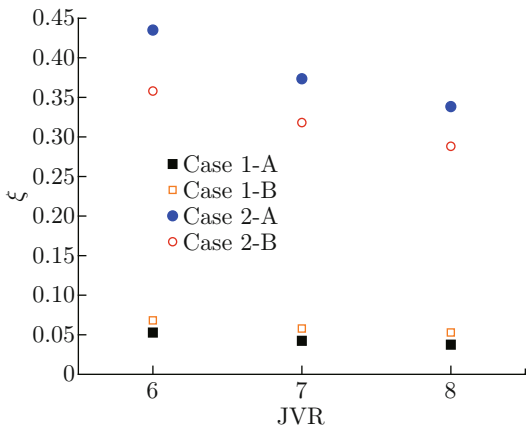

Fig. 7 Non-uniformity of flow under forward and backward conditions

In some practical situations, the impeller shaft has no protected cover and the effect of its rotation cannot be neglected. The shaft's rotational speed is taken as 4 000 r/min in the computations. The surface streamlines at the impeller plane are presented in Fig. 8. The symmetric secondary flows above the shaft in Case 1-B are clearly shown, which can make the flow spiral along the shaft and influence the efficiency of the waterjet pump. In addition, the secondary flows in Case 1-C even become twisted because of the shaft rotation, and the flow patterns near the left and right walls are also affected.

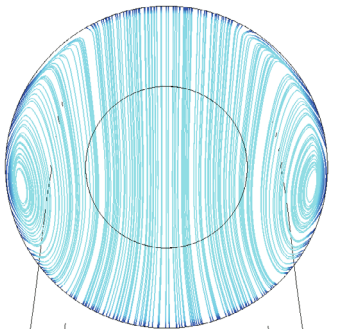

(a) Case 1-A

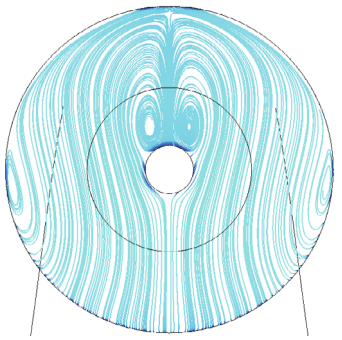

(b) Case 1-B

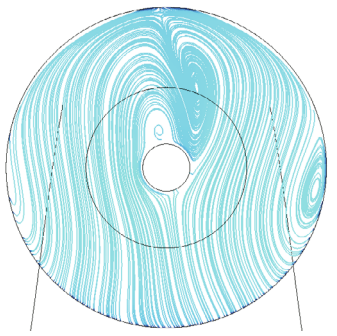

(c) Case 1-C

Fig. 8 Streamlines at the impeller plane at JVR=8

3.2 Backward with/without Reversing Flow

Simulation results of Case 2 and Case 3 are compared to reveal the differences between the backward conditions with and without reversing jet flow. Figure 9 shows the differences in surface pressure of the two cases at JVR = 6, 7, 8. On the ramp side, the pressure coefficients before the 10th tab in Case 3-A are obviously negative when considering the jet flow from the reversing bucket, indicating that the flow field on the ramp side near the duct inlet is improved due to the reversing flow. The peak value becomes lower as JVR increases, which can be found from the change of y-axis magnitude. However, the pressures from the 10th tab to 35th tab in Case 3-A become positive and keep increasing, which is in accordance with the tendency of Case 2-A but with higher values. It illustrates that the reversing jet flow results in more unfavorable pressure

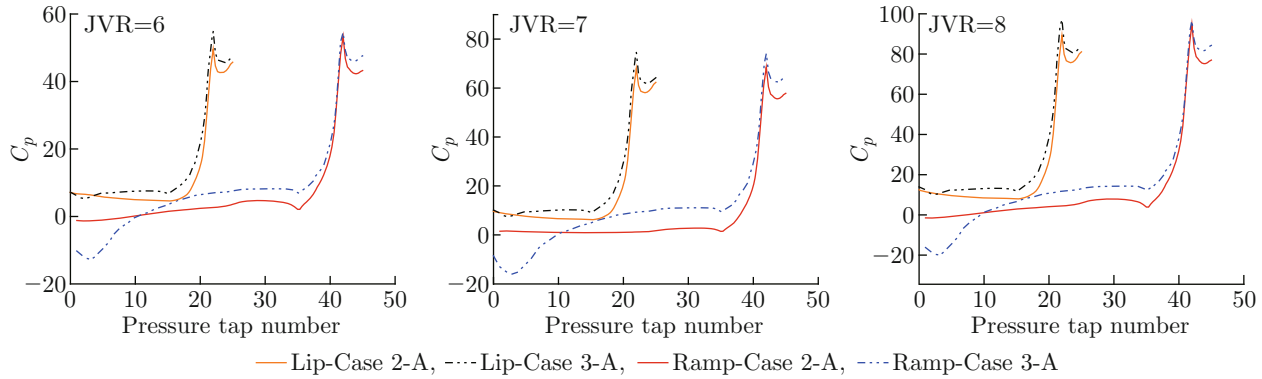

Fig. 9 Pressure distribution under backward conditions

fields for the protection of impellers, and the cavitations are more likely to occur. On the lip side, most surface pressure coefficients in Case 3-A are larger than those in Case 2-A due to the reversing flow. Compared with the ramp side, an obvious difference is that there is no negative coefficient value near the duct inlet on the lip side, but the effect of the reversing jet flow still can be seen from the pressure fluctuation from the 1st tab to 3rd tab.

The contours of static pressure at the impeller plane at JVR=8 are presented in Fig. 10. It can be found from the changes of the pressure under backward conditions that the pressure at the impeller plane in Case 3-B is much higher than that in Case 3-A. This tendency is deserved, because the existence of the impeller shaft leads to the obstruction of the flow around and, consequently, the lower fluid velocity. In addition, the pressure in Case 3-C becomes higher due to the shaft rotation. That is, the flow field under backward conditions with the reversing jet flow is much more sensitive to the presence of the shaft, even when it is stationary. Therefore, it is vital to take also the impeller shaft and its rotation into account in the numerical simulations of the viscous flow within the waterjet intake.

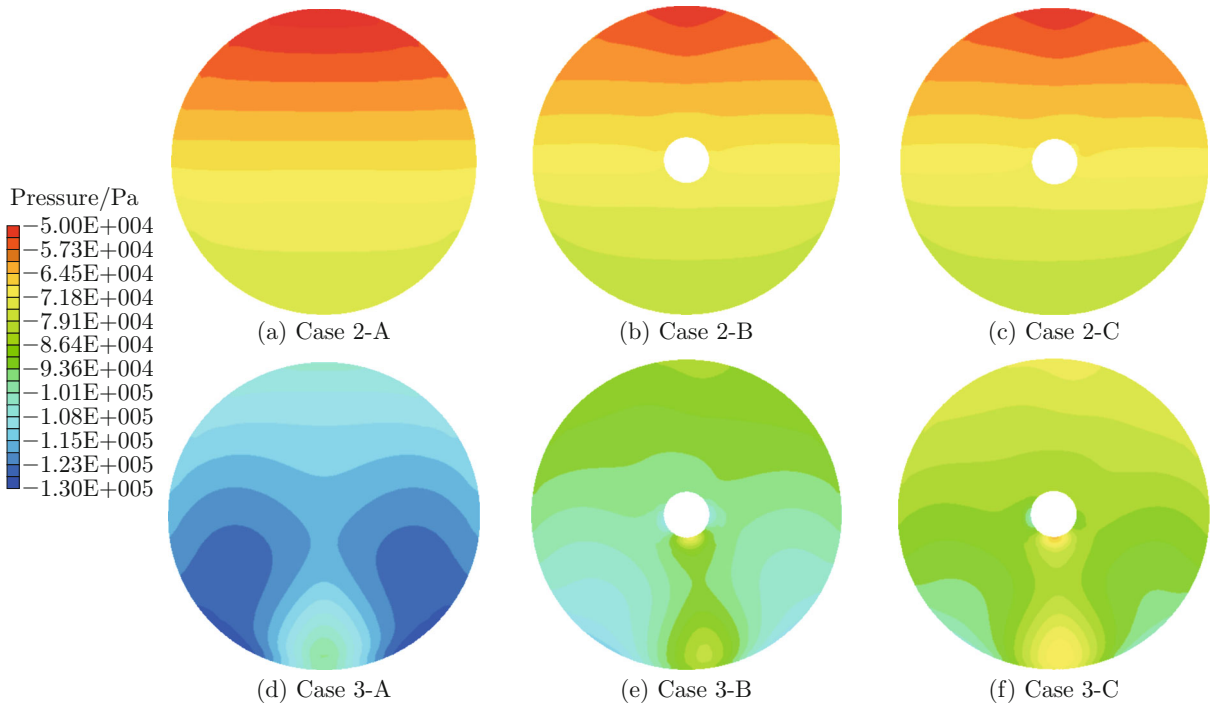

Fig. 10 Pressure contours at the impeller plane at JVR=8

3.3 Forward and Oblique Conditions

In Fig. 11, the simulation results of oblique moving cases are compared with those of forward motion cases in order to analyze the characteristics of flow field. Little differences of surface pressure distribution on the ramp and lip sides are observed, and the

pressure coefficients of total transverse flow (90°) are only slightly larger than those of forward conditions, as shown in Fig. 11(a). However, these results do not represent the whole flow field within the waterjet intake duct. It can be seen from Fig. 11(b) that the non-uniformity of fluid velocity at the impeller plane increases significantly with the increase of the oblique moving angle, indicating that the flow field becomes much more non-uniform under conditions with large angle of oblique motion.

Indeed, the transverse flow across the hull of an oblique moving vessel has a large effect on the flow field at the impeller plane, even at small angles. The pressure contours and surface streamlines at the impeller plane are twisted because of the transverse flow across the intake inlet, as shown in Fig. 12. The secondary flows make the fluid spiral within the intake and into the pump.

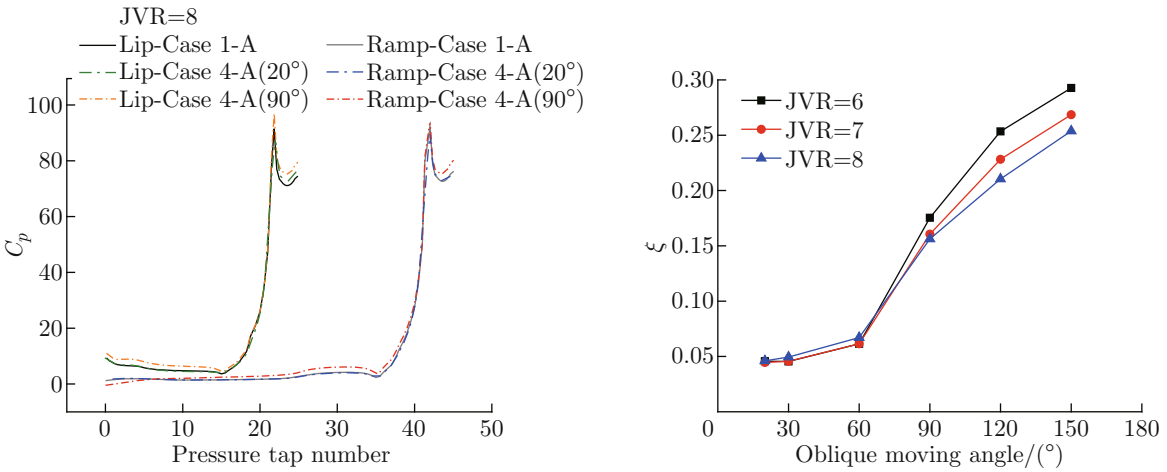

(a) Pressure distribution (b) Non-uniformity

Fig. 11 Simulation results of oblique moving cases

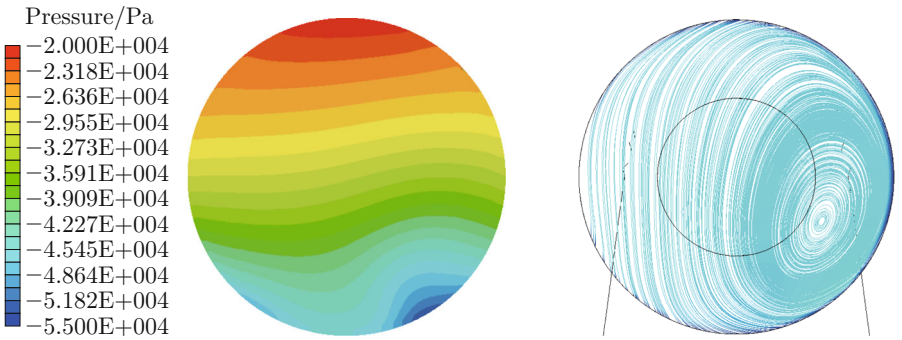

(a) Pressure contours (b) Streamlines

Fig. 12 Flow field under oblique moving condition (20°) at JVR=8

4 Conclusion

By using an RANS solver, the incompressible viscous flow within a flush type of waterjet intake duct is numerically simulated to provide a deep understanding of the complicated flow phenomena under different motion conditions. Therein, the effects of the steering and reversing unit as well as the impeller shaft on the flow field are taken into account. Systematic computations are performed at different jet velocity ratios. By comparing the characteristics of flow fields within the waterjet intake duct, it is found that the static pressure around the impeller plane under backward conditions with the effect of the reversing jet flow is the lowest, which indicates that the flow field is the worst for the impeller, and the cavitations are most likely to occur. The flow field under forward conditions is less uniform because of the presence of the shaft, while the velocity uniformity under backward conditions is improved. The rotation of the shaft causes the asymmetric secondary flow above the shaft under all conditions. The pressure contours under backward conditions with the reversing jet flow are sensitive to the presence of the shaft.

The numerical results demonstrate that the characteristics of the viscous flow within the waterjet intake

duct vary under different motion conditions. It suggests that more considerations, such as the effects of the shaft and the steering and reversing unit, should be taken into account in the prediction of hydrodynamic performance of the waterjet intake. The present study can provide a certain reference for the design optimization of waterjet propulsion system.

References

[1] CARLTON J S. Marine propellers and propulsion [M]. 3rd ed. Oxford, UK: Elsevier Ltd., 2012.

[2] VERBEEK R, BULTEN N. Recent development in waterjet design [C]//*Proceedings of International Conference on Waterjet Propulsion II*. Amsterdam, the Netherlands: RINA, 1998.

[3] DING J M, WANG Y S. Research on flow loss of inlet duct of marine waterjets [J]. *Journal of Shanghai Jiao Tong University* (*Science*), 2010, **15**(2): 158-162.

[4] ITTC. The specialist committee on validation of waterjet test procedures: Final report and recommendations to the 23rd ITTC [C]//*Proceedings of the 23rd ITTC*, *Volume 2*. Venice, Italy: ITTC, 2002: 379-407.

[5] ITTC. The specialist committee on validation of waterjet test procedures: Final report and recommendations to the 24th ITTC [C]//*Proceedings of the 24th ITTC*, *Volume 2*. Edinburgh, UK: ITTC, 2005: 471-508.

[6] VON ELLENRIEDER K. Free running tests of a waterjet propelled unmanned surface vehicle [J]. *Journal of Marine Engineering & Technology*, 2013, **12**(1): 3-11.

[7] BULTEN N. A breakthrough in waterjet propulsion systems [C]//*Proceedings of the International Maritime Defence Exhibition and Conference*. Doha, Qatar: DIMDEX, 2008: 1-6.

[8] DING J M, WANG Y S. Parametric design and application of inlet duct of marine waterjet [J]. *Journal of Shanghai Jiao Tong University*, 2010, **44**(10): 1423-1428 (in Chinese).

[9] PARK W G, YUN H S, CHUN H H, et al. Numerical flow simulation of flush type intake duct of waterjet [J]. *Ocean Engineering*, 2005, **32**(17/18): 2107-2120.

[10] BULTEN N, VAN ESCH B. Review of thrust prediction method based on momentum balance for ducted propellers and waterjets [C]//*Fluids Engineering Division Summer Meeting*. Houston, USA: ASME, 2005: 1621-1629.

[11] BULTEN N. Numerical analysis of a waterjet propulsion system [D]. Eindhoven, the Netherlands: Eindhoven University of Technology, 2006.

[12] ESLAMDOOST A. The hydrodynamics of waterjet/hull interaction [D]. Gothenburg, Sweden: Chalmers University of Technology, 2014.

[13] JUNG K H, KIM K C, YOON S Y, et al. Investigation of turbulent flows in a waterjet intake duct using stereoscopic PIV measurements [J]. *Journal of Marine Science and Technology*, 2006, **11**(4): 270-278.

[14] XU H L, ZOU Z J. Numerical simulation of the viscous flow in a waterjet intake duct under backward conditions [C]//*Proceedings of the 27th International Ocean and Polar Engineering Conference*. San Francisco, USA: ISOPE, 2017: 1073-1078.